THE PENNSYLVANIA STATE UNIVERSITY
SCHREYER HONORS COLLEGE

DEPARTMENT OF CHEMICAL ENGINEERING

CHARACTERIZATION OF CHAIN ALIGNMENT AT BURIED INTERFACES USING VARIABLE-ANGLE SPECTROSCOPIC MUELLER MATRIX ELLIPSOMETRY

BRYAN HENRY SMITH
SPRING 2018

A thesis
submitted in partial fulfillment
of the requirements
for a baccalaureate degree
in Chemical Engineering
with honors in Chemical Engineering

Reviewed and approved* by the following:

Enrique D. Gomez
Associate Professor of Chemical Engineering
Thesis Supervisor

Darrell Velegol
Distinguished Professor of Chemical Engineering
Honors Adviser

* Signatures are on file in the Schreyer Honors College.

ABSTRACT

Thin semiflexible polymer films are of great interest to organic electronics and other technologies. Theory and simulations predict that the alignment layer in semiflexible polymers scales with chain stiffness. However, the thickness of this aligned layer at the buried interface is challenging to characterize directly. Using Mueller matrix variable angle spectroscopic ellipsometry, we have modeled the optical response of regiorandom poly(3-hexylthiophene) P3HT in order to extract the aligned layer thickness. We find that by approximating the optical properties of the aligned layer as regioregular P3HT, the data can be effectively modeled. An aligned layer with thickness on the order of predictions in previous work is detected in regiorandom P3HT films greater than 150 nm while thinner films exhibit greater birefringence. The regiorandom P3HT films were all found to exhibit a degree of optical uniaxial anisotropy.

TABLE OF CONTENTS

LIST OF FIGURES

LIST OF TABLES

ACKNOWLEDGMENTS

I would like to thank my thesis supervisor and mentor Dr. Enrique Gomez for his patience, advice, and unwavering support throughout my time in his research group. I am also extremely grateful for the ellipsometry expertise and assistance from Dr. Nikolas Podraza; it was an honor to collaborate with and learn so much from him. These many thanks are of course extended to my advisor Dr. Darrell Velegol, whose years of academic and career advice helped me to navigate through difficult decisions.

I would also like to acknowledge some other fantastic researchers who took time out of their busy schedules to help me with this research project and others. Thank you very much to Melissa Aplan, Youngmin Lee, and Josh Litofsky for putting up with my years of questions and for mentoring me when I first joined the Gomez group. Many thanks to Dipendra Adhikari for his hospitality and assistance with data collection at the University of Toledo, Carina Bronnbauer for her mentorship at the Friedrich-Alexander University of Erlangen, and to Thinh Le for his help with polymer characterization. Finally, thank you to Douglas Kushner for introducing me to ellipsometry.

Dr. Michael Janik, Dr. Raymond Funk, Dr. Bratoljub Milosavljevic, Dr. Kathlene Baldanza, and Mr. Gregory Somers deserve recognition as well, because without their courses and assistance, my engineering, chemistry, math, and critical thinking skills would be insufficient to complete this honors thesis.

Last but not least, I would like to thank my family and friends for supporting me throughout my undergraduate studies. I am grateful for your many words of support in stressful times and could not have even reached half of my potential without you all.

Chapter 1: Introduction

Motivation

The objective of this thesis is to characterize chain alignment at the buried semiflexible polymer substrate interface. Polymers play an increasingly important role in a broad range of new technologies. While traditionally used as building, structural, and packaging materials, polymers are found in electronics, sources of clean energy, membranes, and biomedical devices. Understanding and controlling polymer morphology is key to engineering these applications.

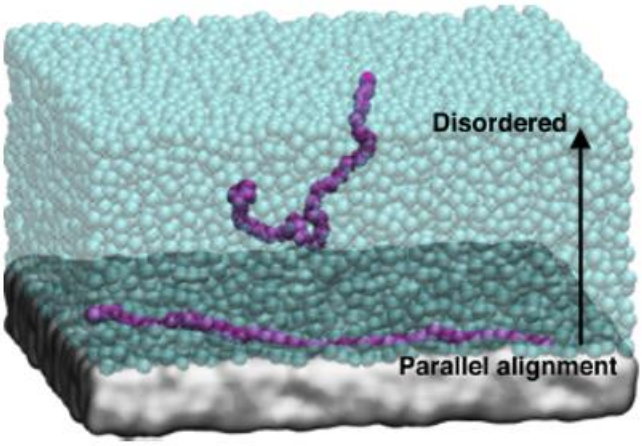

Figure 1. Chain alignment at the buried polymer-substance interface.[1]

Theory and simulations predict that the alignment layer in semiflexible polymers scales with chain stiffness, which is quantified using the persistence length L_p .[1, 2] Figure 1 shows an example of the predicted chain alignment.

Such alignment promotes charge mobility in organic thin film transistors.[1, 3] Polymer chain alignment may improve adhesion or alter membrane transport in some cases.[4, 5] In addition to organic electronics, semiflexible polymers are found in fuel cell membranes and biopolymer

systems.[6, 7] The ability to quickly and non-destructively analyze a wide range of buried interfaces can further the fundamental understanding of the morphology present in many polymer technologies with positive impacts on the environment.

Polymer thin-film Morphology

Polymer morphologies, and therefore properties, are ultimately determined by the interactions that occur between polymer chains. A polymer is considered flexible if the polymer chains freely rotate. Flexible polymer properties are determined by entropic tension, a force that acts to maximize possible chain conformations. Many common polymers including polyethylene are classified as such. Stiff polymers are polymers with chains that are limited in movement by a bending energy; there is an enthalpy barrier to motion that decreases with higher temperature. Very stiff polymers have chains that behave like rigid rods.

Some polymers are best classified as semiflexible because whether the chains behave as flexible or stiff depends on the length of the chain or segment being considered. This has significant implications on how the polymer behaves and on how the polymer should be modeled. Persistence length, L_p, is the parameter that quantifies the length scale below which the polymer acts stiff in the sense that chain motion is restricted by the bending energy. L_p in monomer units is defined in Equation 1 for a 3 dimensional system, where T is temperature, κ is bending rigidity, and k_B is the Boltzmann constant.

$$L_p = \frac{\kappa}{k_B T} \tag{1}$$

Above the persistence length, the polymer chains can be considered flexible with independent segments on the order of L_p, and polymers with a persistence length on the order of other

important scale lengths can be classified as semiflexible.[8] Semiflexible polymers are frequently found in biological systems, but are also found in the field of organic electronics. Semiflexibility, or backbone rigidity, can arise from steric effects, bonding, or electronic delocalization within the polymer.[2]

Theory and simulation has been developed to properly predict and explain the interfacial behavior of these materials. Morse and Fredrickson outline a self-consistent-field theory to analyze these systems based on the wormlike chain model rather than a Gaussian model used to describe fully flexible systems.[2] A key prediction of this model is that semiflexible polymer chains will align parallel to an interface between incompatible semiflexible polymers.[2] Using a similar approach, Chen, Sullivan, and Yuan predict parallel alignment to an impenetrable surface for a polymer chain confined to a narrow slit.[9, 10] Ivanov et. al use Monte Carlo simulation variants to predict that impenetrable surfaces induce nematic order in semiflexible athermal polymer solutions.[11]

Zhang et. al use molecular dynamics simulations of bead-spring chains to estimate the thickness of a spontaneously aligned layer at the interface of a polymer melt and impenetrable substrate.[1] This study finds that the thickness is approximately L_p.[1] A lattice version of self-consistent field theory is used to predict that nematic coupling increases the interface alignment thickness.[1] The work described in this manuscript seeks to test the prediction made by Zhang et. al by characterizing the thickness of the alignment layer in semiflexible polymer film samples.

Ellipsometry

Interface induced alignment has been detected in semiflexible polymer samples. Kline et. al use X-ray diffraction rocking curves to provide evidence for highly oriented crystals at the buried interface between various polythiophenes and substrates used in thin film transistor devices.[3] Xiao et. al use sum frequency generation vibrational spectroscopy to probe similar systems and conclude that the hydrophobicity of the polythiophene sidechains affects the orientation of the thiophene ring near interfaces.[12] Ellipsometry, however, is best suited to test the predictions made by Zhang et. al because of its common use in determining the thicknesses of multiple thin layers within a film stack. The optical properties of a polymer film are in part determined by morphology. Optical birefringence is considered a relative measure of chain orientation.[13, 14] The optical birefringence as determined from ellipsometry will therefore be used to probe the chain alignment throughout semiflexible polymer films and at the buried polymer-substrate interface.

Ellipsometry is a technique involving the generation and analysis of polarized light. Polarized light is directed at a thin film, and changes to the polarization state of the light reflected by the film are analyzed in order to gain information about the optical properties of the film. In spectroscopic ellipsometry, two independent quantities, psi (Ψ) and delta (Δ), are measured at each wavelength allowing more information to be collected than in other similar methods.[15] These quantities describe the change in complex Fresnel coefficients as light interacts with the sample, with $\tan(\Psi)$ being the amplitude ratio and Δ being the phase shift.[15] To determine the optical properties and thicknesses of layers in a film stack, the raw data must be fit to a model using ellipsometry modeling software such as the CompleteEase software package from J.A. Woollam. The optical properties are modeled using oscillators to describe the

refractive index and absorption coefficient functions, which are related by the Kramers-Kronig relationship.[16] The Kramers-Kronig relationship is shown in Equation 2 where ε_1 is the refractive index,ε_2 is the absorption coefficient, E is photon energy, and P is the principal part of the integration.

$$\varepsilon_1(E) = 1 + \frac{2}{\pi}\int_0^{\infty} \frac{E'\varepsilon_2(E')}{E'^2 - E^2} dE' \quad (2)$$

When analyzing samples with a complex optical response, Mueller matrix ellipsometry is preferred. This advanced ellipsometry variant is necessary for accurate characterization of anisotropic or depolarizing samples.[15, 17] A Mueller matrix is a 4 x 4 matrix used in the Stokes-Mueller representation to fully describe the transformation of polarized light caused by a sample.[16] In order to measure all 16 Mueller elements, the ellipsometer must be capable of generating and analyzing 4 basis states of polarized light.[22] The J. A. Woollam RC2 is one such commercially available instrument.

Hypothesis

If certain reasonable assumptions are made about the optical response of a semiflexible polymer film, ellipsometry should be able probe the buried interface and provide information on the nature of a predicted aligned layer. If the aligned layer is present, the optical property model should fit the collected data better than a more traditional model. Films of various thickness will be analyzed to test if the interface thickness and bulk order in the film changes with total film thickness.

The semiflexible polymer studied in this research is poly(3-hexylthiophene) or P3HT. Polythiophenes are popular research materials for organic electronics due to their easy processability, high conductivity, and variety of established synthesis routes.[18] The regioregular P3HT is known to be semicrystalline with crystallites that align parallel to substrates, whereas regiorandom P3HT is mostly

isotropic.[19] The structure of these polymers is shown in Figure 2. Mueller matrix ellipsometry will be used to characterize the optical properties of regiorandom P3HT films of various thicknesses and explore various models including those that take into account the possibility of an aligned layer at the buried polymer-substrate interface. Optical properties derived from regioregular P3HT will be used as the properties of the aligned layer. Ultimately, the prediction in Zhang et. al that P3HT exhibits a 4.5 nm thick aligned layer at the buried interface will be tested.[1]

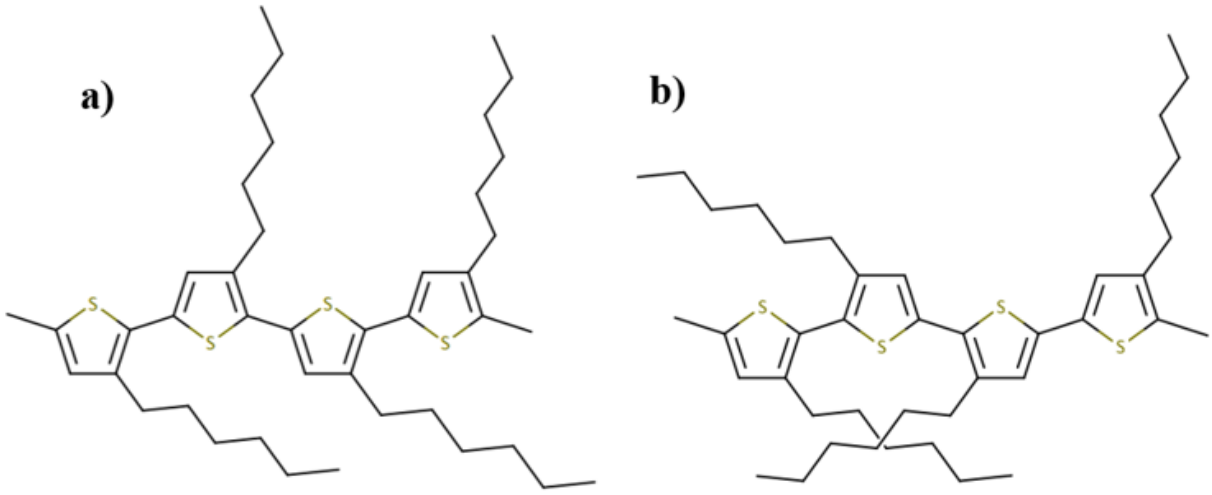

Figure 2. a) Regiorandom P3HT and b) regioregular P3HT structure

Chapter 2: Materials and Methods

Sample Preparation

Solutions of regiorandom P3HT (58% regioregular, M_w = 155 kg/mol, Sigma-Aldrich) and regioregular P3HT (95% regioregular, M_w = 17.5 kg/mol) were made with anhydrous chlorobenzene (Sigma-Aldrich) in a N_2 glove box. Solutions were stirred for a minimum of 8 hours at room temperature prior to use.

Thin film samples were created by spin coating on approximately 1 cm^2 pieces of silicon wafer with native oxide. Substrates were cleaned by sonication in acetone for 10 minutes followed by isopropanol for 10 minutes and then 10 minutes of UV ozone treatment. Polymer solutions were cast in a N_2 glove box at 1000 rpm for 1 minute and then annealed for a minimum of 8 hours at 165 °C to allow the film to dry and equilibrate.

Table 1 lists the regiorandom samples modeled for this study, and Table 2 lists the regioregular samples modeled.

Table 1. Utilized regiorandom P3HT data. Various subsets of this data are considered for different analyses throughout the thesis as indicated.

Approximate film thickness (nm)	Samples	Data collection locations per film
24	3	2
37	3	2
65	2	2
101	3	2
154	3	2
229	4	2

Table 2. Utilized regioregular P3HT data. This data will be use to create an accurate model for regioregular P3HT that will be used in the analysis of regiorandom P3HT as described later in this thesis.

Approximate film thickness (nm)	Samples	Data collection locations per film
14	1	1
18	1	1
24	1	1
25	1	1
49	1	1

Data Collection

Ellipsometry data was collected on a J. A. Woollam RC2 ellipsometer. Regiorandom P3HT data was collected at the University of Toledo and regioregular P3HT data was collected at the Pennsylvania State University, University Park. Data was collected in Mueller Matrix mode from 210 nm to 1690 nm. Regiorandom P3HT data was obtained at 50°, 60°, and 70° incident angles with a 30 second data collection time.

Data was collected from at least 2 locations on each of the regiorandom P3HT films. Samples were rotated 90 degrees between measurements to accomplish this. Overlap between the measurement regions were minimized but unavoidable.

Blank silicon with native oxide wafers were run with each data collection. This data was used to extract the native oxide thickness for the wafers used to make the polymer films. Typical oxide thickness was on the order of 1-2 nm.

Modeling

All data modeling was carried out in CompleteEase. A variety of models were used to fit the data. Figure 3 shows the one and two polymer layer strategies for modeling a polymer film on top of the silicon with native oxide substrate.

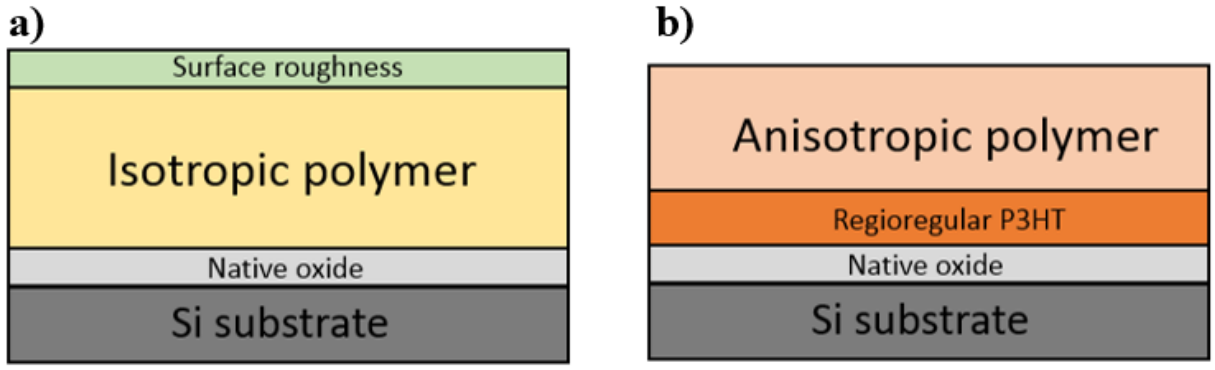

Figure 3. Two possible models for regiorandom P3HT

a) An isotropic one-polymer layer model that accounts for surface roughness. b) A two-polymer layer model with an anisotropic top layer and bottom layer with fixed optical properties matching regioregular P3HT. This model does not account for surface roughness.

Layers were modeled as having either isotropic or uniaxial anisotropic optical properties. In the uniaxial anisotropic models, the x and z plane were considered to have a different optical response and therefore set of optical properties. Optical properties associated with the x plane are referred to as ordinary, while z plane properties are referred to as extra-ordinary.

Models were used to fit either a group of data collected from all samples of a given thickness, one set of data from samples of each thickness, or just one individual data set. The models referred to in each figure in this thesis are summarized in Table 1. Regioregular and regiorandom data sets were analyzed separately.

Table 3. Ellipsometry models used to acquire data presented in various figures.

Figures	Top Layer	Bottom Layer	Data being fit
4a, 5	Isotropic	None	One data set of each thickness
4b, 6	Anisotropic	None	One data set of each thickness
7	Anisotropic	None	All data sets of one thickness
8, 9, 10, 11	Anisotropic	None	Each data set individually
12	Anisotropic	Anisotropic regioregular P3HT	All data sets of one thickness
13, 14, 15, 16, 17, 18	Anisotropic	Anisotropic regioregular P3HT	Each data set individually
19	Isotropic	Anisotropic regioregular P3HT	Each data set individually

Polymer optical properties were modeled with Gaussian and Tauc-Lorentz oscillators, with each set of properties containing between 3 and 7 oscillators. Oscillators were added or removed as necessary depending on what data was being fit. Generally, thinner films required fewer oscillators. The substrate in each model was accounted for using silicon with native oxide properties provided in the CompleteEase software. The native oxide thickness was not fit while modeling the polymer films and was held to a value determined by fitting the blank wafers. All models were run until they converged or for 10,000 iterations.

Surface roughness was modeled as a 50% Bruggeman effective medium approximation (EMA) between the top polymer layer optical properties and void. Depolarization was set at 33.3%, the CompleteEase default for EMA-coupled layers. This layer was added at the top of the layer stack as shown in Figure 3a.

Chapter 3: Discussion and Results

Regiorandom P3HT films of various thicknesses were prepared from solutions of various concentrations. One set of data from each total film thickness was first simultaneously fit with a single layer isotropic model. This model reflects a simplistic but plausible morphology for disordered regiorandom polymer films. As shown in Figure 4a, the model poorly describes diagonal Mueller matrix elements in the P3HT absorption region for thicker films. This result strongly suggests that there is some degree of optical anisotropy and therefore order in the system. The optical properties derived from this model are shown in Figure 5.

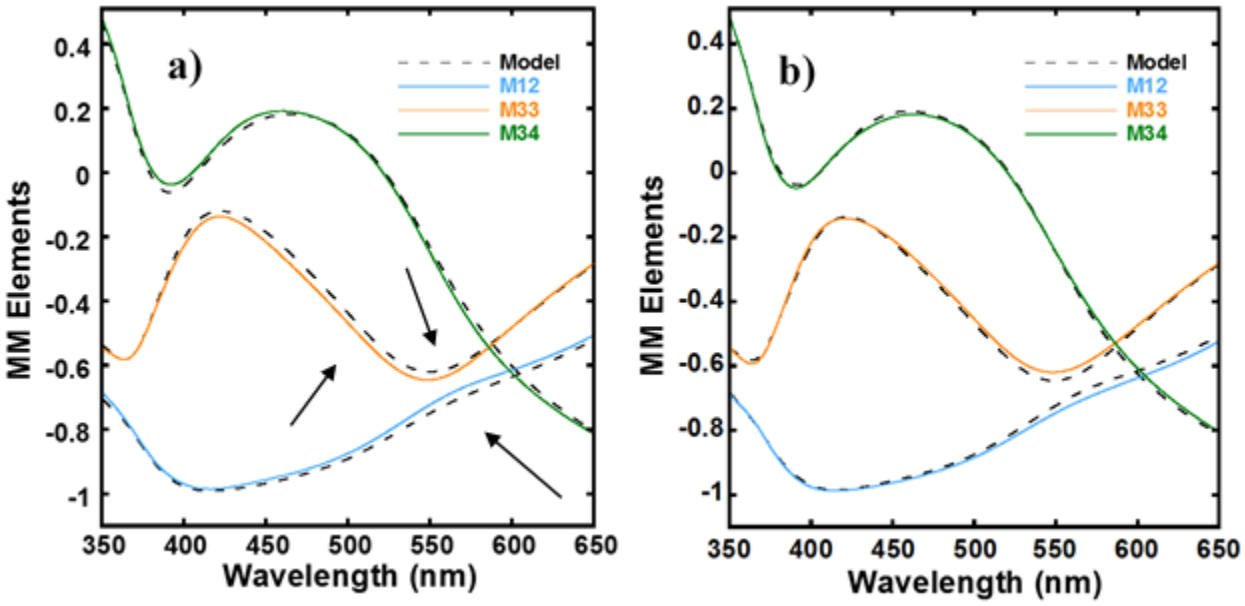

Figure 4. Selected Mueller matrix elements fit with one-layer models that assume constant optical properties for multiple film thicknesses.

Selected Mueller matrix elements for a 155 nm thick regiorandom P3HT film at 60° incident angle in the 350-650 nm range are shown as solid lines. A one-layer model shown as dashed lines was derived from fitting data in the 210-1690 nm wavelength range for a variety of film thicknesses (24-230 nm) with the same optical properties. a) The optical properties are assumed to be isotropic. Arrows highlight that the fit is not optimal in the 500-600 nm range for M12 and M33. b) The optical properties are assumed to be anisotropic which leads to a slightly improved fit which justifies adding further complexity to more accurately describe the film.

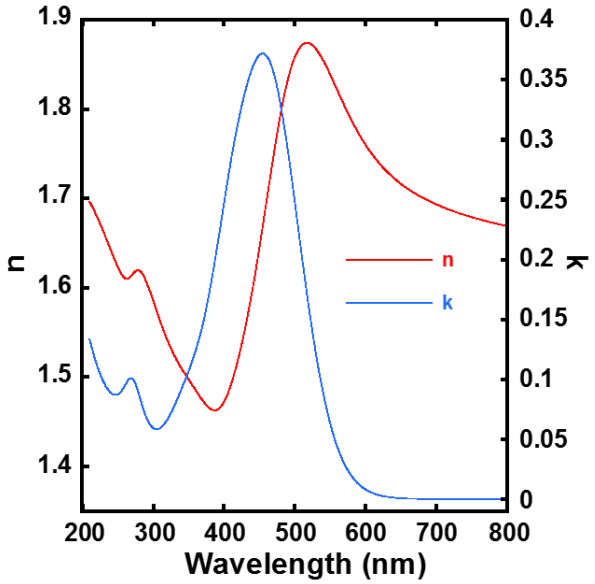

Figure 5. Isotropic regiorandom P3HT optical properties

Regiorandom P3HT optical properties derived from fitting a one-layer isotropic model to data in the 210-1690 nm range for a variety of film thicknesses (24-240 nm) all assumed to have the same optical properties. Refractive index (n) and absorption coefficient (k) are plotted. These properties fully describe the film at all depths and at all angles of incident in this model.

A single layer anisotropic model was subsequently fit to the same data. As shown in Figure 4b, this change significantly improves the fit quality although discernable discrepancies exist in M12 and M33 around 550 nm. The optical properties derived from this model are shown in Figure 6. The birefringence exhibited at most wavelengths indicates some degree of ordering within some of the films.

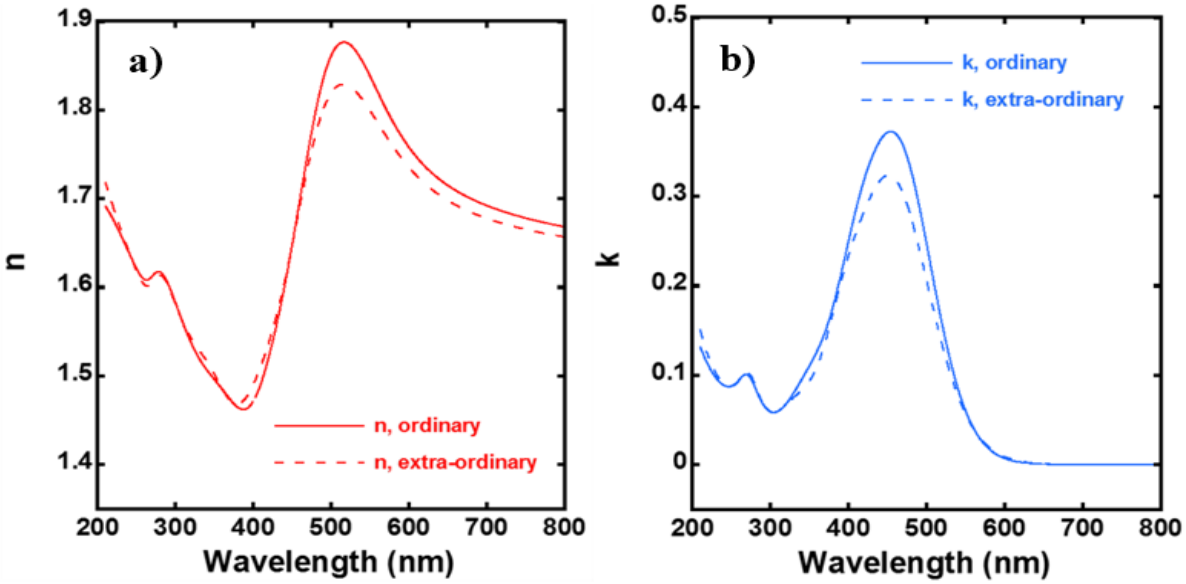

Figure 6. Anisotropic regiorandom P3HT optical properties

Regiorandom P3HT optical properties derived from fitting a one-layer anisotropic model to data in the 210-1690 nm range for a variety of film thicknesses (24-240 nm) all assumed to have the same optical properties. a) Ordinary and extra-ordinary refractive index (n). b) Ordinary and extra-ordinary absorption coefficient (k). These properties describe the model at all depths.

To investigate the relationship between birefringence and film thickness, a single layer anisotropic model was simultaneously fit to all data collected from the approximately 154 nm thick samples. Figure 7 demonstrates the improvement of this fit over the fits shown in Figure 4. This suggest that an optimal model must consider a change in optical properties with thickness.

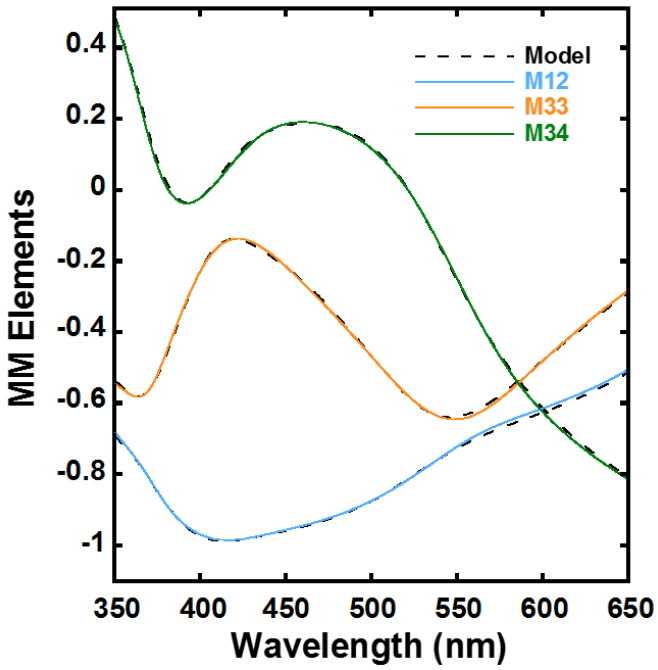

Figure 7. Selected Mueller matrix elements fit with an anisotropic one-layer model

Selected Mueller matrix elements for a 155 nm thick regiorandom P3HT film at 60° incident angle in the 350-650 nm range shown as solid lines. A one-layer anisotropic model shown as dashed lines was derived from fitting data in the 210-1690 nm wavelength range for all 155 nm samples with the same optical properties. This fit improvement justifies considering models in which properties change with thickness.

To quantify the relationship between birefringence and thickness, single layer anisotropic models were fit to each data set collected. The possibility of surface roughness was included in these models to rule out interference from any roughness that was likely present. The roughness values determined from these models are plotted in Figure 8. Figure 9 shows the birefringence results from this analysis. This wavelength is selected because the samples exhibit no absorption and low depolarization at this wavelength, and it is representative of the entire low energy portion of the birefringence spectrum.

There is a statistically significant decrease in birefringence between the thickest two samples and the thinner samples. Statistical significance was determined using a two-tail p-test that does not assume equal variance. The conventional p value of 0.05 was chosen as the

significant cut off, and pairs for which the p value is less than 0.01 are marked as having even more likely significance. The standard deviations for this measurement decrease dramatically with thickness, with the 24 nm samples likely being too thin to model with any significant sensitivity to birefringence.

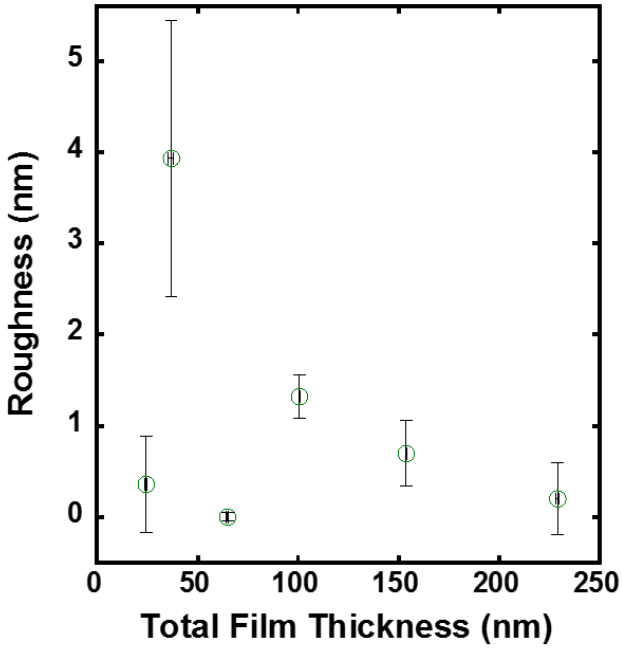

Figure 8. Mean surface roughness shown with standard deviation bars for regiorandom P3HT films of various thickness as determined using the one-layer anisotropic model

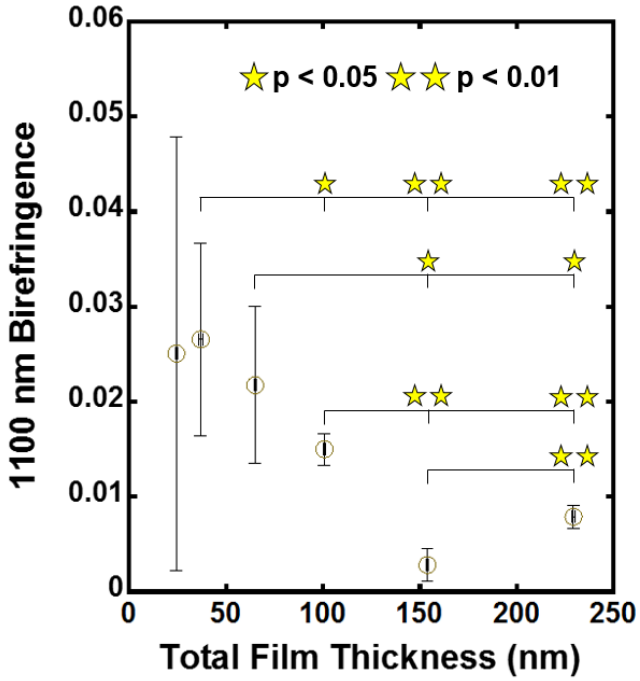

Figure 9. Mean 1100 nm birefringence shown with standard deviation bars for a one-layer ansiotropic model

Mean 1100 nm birefringence shown with standard deviation bars for regiorandom P3HT films of various thickness as determined using a single layer anisotropic ellipsometry model that accounts for surface roughness. The thickest two sets of samples show statistically significantly reduced birefringence as compared to thinner sets of samples. Statistically different pairs are annotated with stars.

This analysis was repeated without accounting for roughness as shown in Figure 10. The most significant change occurs in the 38 nm samples, which were also found to be the roughest samples. However, the 154 nm and 230 nm samples are still found to have greater birefringence than the 100 nm and 66 nm films.

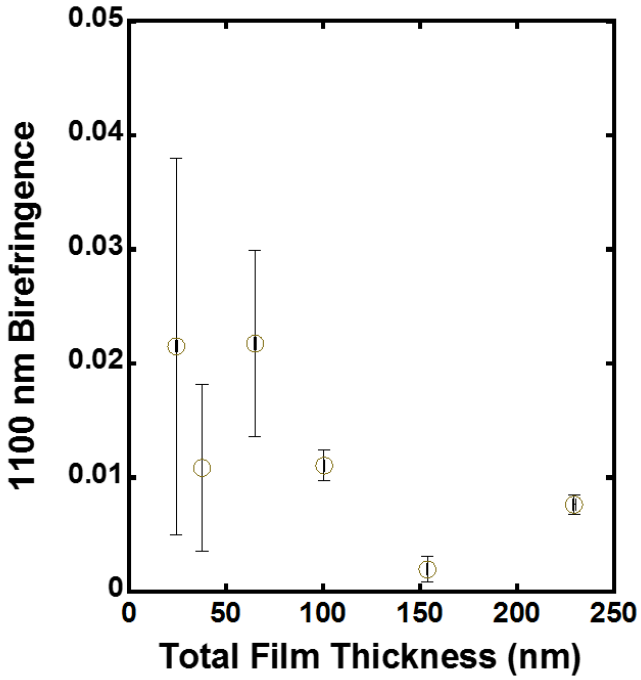

Figure 10. Mean 1100 nm birefringence results from a single layer anisotropic ellipsometry model that does not account for surface roughness

Mean 1100 nm birefringence results from a single layer anisotropic ellipsometry model that does not account for surface roughness. The general trend in the data is similar to that of Figure 11, although the 38 nm data point has lower birefringence in this analysis.

To investigate of surface induced chain alignment contributes to the birefringence detected, a second anisotropic layer was added to the models. This bottom layer was assigned fixed optical properties matching those derived from simultaneously modeling regioregular P3HT with a single anisotropic layer. Regioregular P3HT is semicrystalline and therefore exhibits much higher birefringence than amorphous regiorandom P3HT. Although chain alignment and crystallization are not synonymous, it is expected that both ordering processes will result in relatively higher birefringence.[13, 14] It was found that the two layer models were not sensitive enough to independently derive physically realistic optical properties for the bottom layer, necessitating this assumption. The derived regioregular P3HT optical properties are shown in Figure 11.

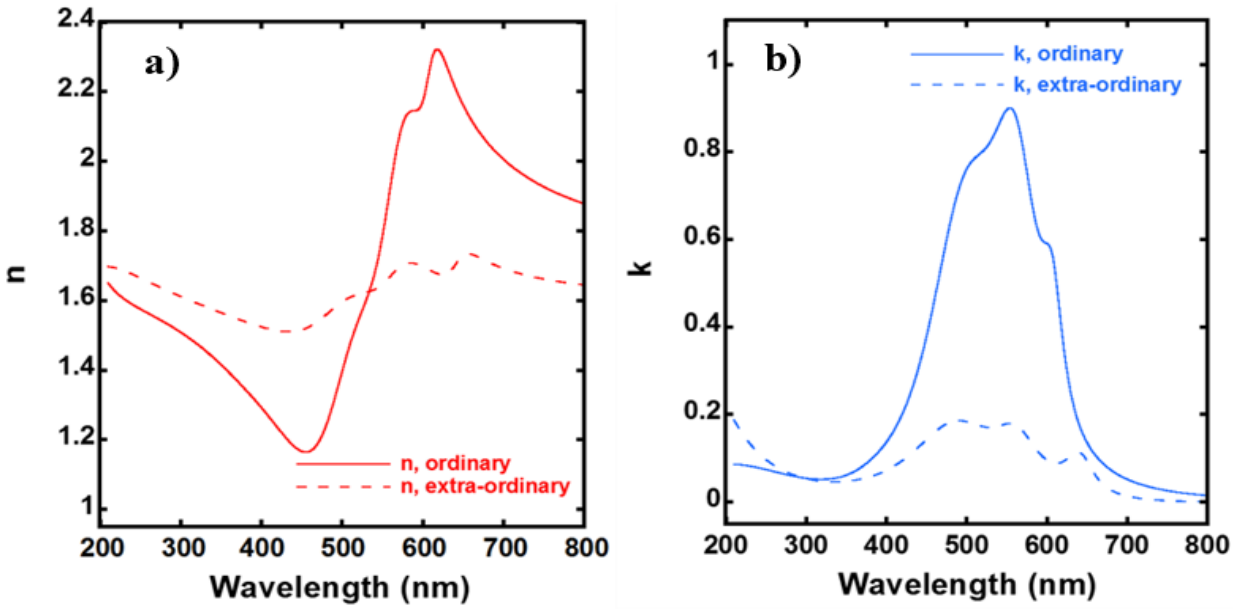

Figure 11. Regioregular P3HT optical properties

Regioregular P3HT optical properties derived from fitting a one-layer anisotropic model to data in the 210-1690 nm range for a variety of film thicknesses (14-49 nm) all assumed to have the same optical properties. These properties are used in the buried aligned interface layer for the two layer anisotropic models. a) ordinary and extra-ordinary refractive index (n). b) ordinary and extra-ordinary absorption coefficient (k).

A two-layer anisotropic model was simultaneously fit to all data collected from the approximately 154 nm thick samples. The bottom layer optical properties were fixed as the previously derived regioregular P3HT properties, while both layer thicknesses and the top layer optical response were allowed to be fit. Figure 12 demonstrates the improvement of this fit over the fits shown in Figure 4 and 7, while Table 4 shows the improvement in unweighted mean squared error (MSE) between the fits shown in Figure 4a, 4b, 7, and 12 over the 350-650 nm range for Mueller elements M12, M33, and M34.

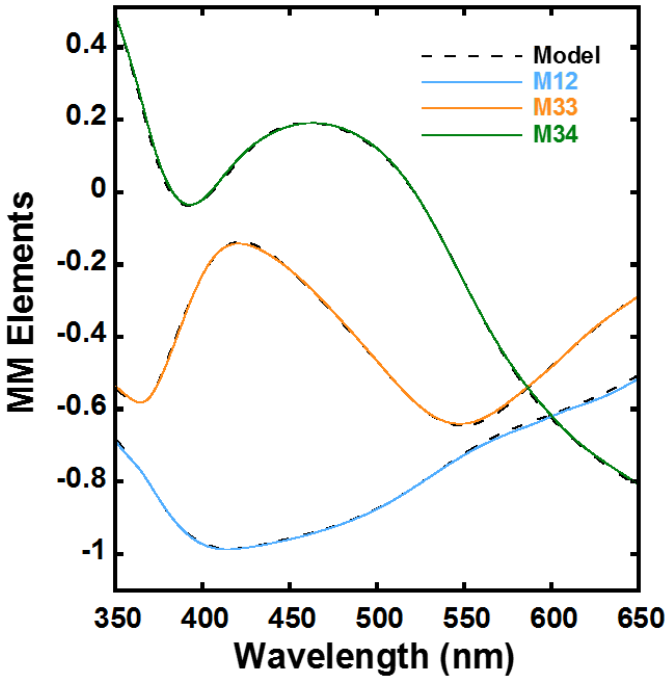

Figure 12. Selected Mueller matrix elements for a 155 nm thick regiorandom P3HT film at 60° incident angle in the 350-650 nm range shown as solid lines

Selected Mueller matrix elements for a 155 nm thick regiorandom P3HT film at 60° incident angle in the 350-650 nm range shown as solid lines. A two-layer anisotropic model shown as dashed lines was derived from fitting data in the 210-1690 nm wavelength range for all 155 nm samples with the same optical properties. This model fits slightly better than the equivalent one layer model.

Table 4. Unweighted MSE in the 350-650 nm absorption region for selected Mueller elements for various models

Figure in which model is portrayed	**Unweighted MSE (x 10^3)**
4a	16.0
4b	10.7
7	5.1
12	3.8

The Equation 3 is used to calculate unweighted MSE where M_{exp} is the experimentally measured Mueller matrix element at a given wavelength, M_{fit} is the model Mueller matrix element at that wavelength, and n is the number of wavelengths data is collected at:

$$MSE = \frac{1}{n}\sum_{i=1}^{n}\sqrt{(M_{exp} - M_{fit})^2} \qquad \text{Equation (3)}$$

The weighted MSE calculated by CompleteEase is typically three orders of magnitude larger than the unweighted MSE, and in this work always refers to all Mueller elements and the entire spectral range.

To quantify the relationship between top layer birefringence and thickness using this model, two-layer anisotropic models were fit to each data set collected. Figure 13 plots top layer birefringence vs. total film thickness when roughness is included in the model. The results are similar to the corresponding results for the single layer model. Regardless of the inclusion of surface roughness, the 154 nm and 230 nm samples have significantly reduced 1100 nm birefringence as compared to thinner samples.

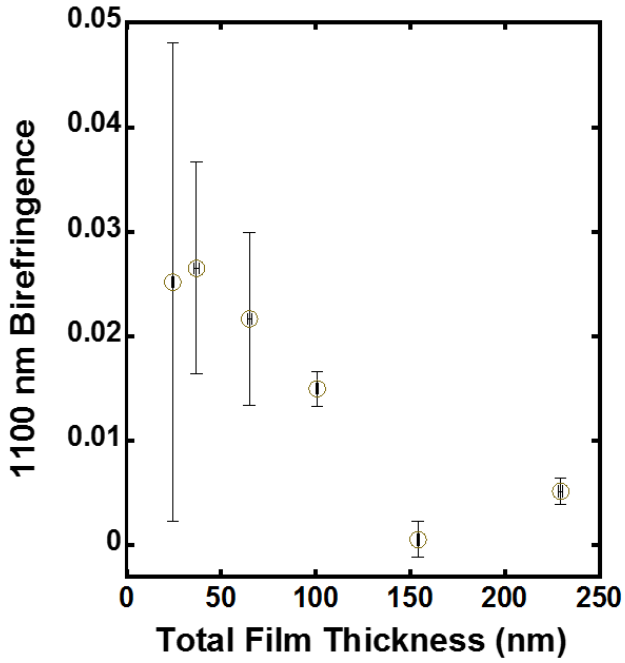

Figure 13. Mean 1100 nm birefringence shown with standard deviation bars for a two-layer anisotropic model that accounts for surface roughness

Mean 1100 nm birefringence shown with standard deviation bars for regiorandom P3HT films of various thickness as determined using a two-layer anisotropic ellipsometry model that accounts for surface roughness. The thickest two sets of samples show statistically significantly reduced birefringence as compared to thinner sets of samples.

Figure 14 shows that as with the one-layer anisotropic models, the addition of surface roughness does not meaningfully change the conclusion, although p values do increase for several pairs. Figure 15 shows the roughness values associated with this analysis.

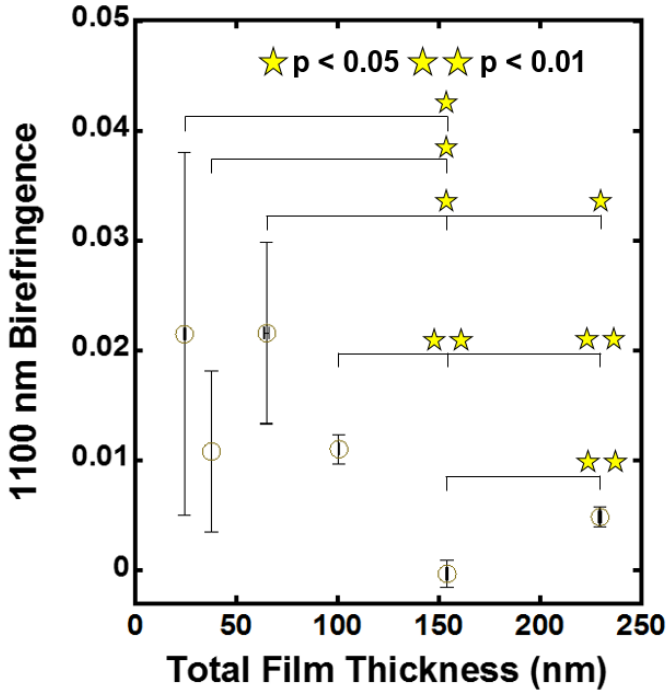

Figure 14. Mean 1100 nm birefringence results for the two-layer anisotropic model that does not account for surface roughness

Mean 1100 nm birefringence results from a two-layer anisotropic ellipsometry model that does not account for surface roughness. The general trend in the data is similar to that of Figure 13, although the 38 nm data point has lower birefringence in this analysis. As in Figure 9, there is a statistical difference between the thickest two data points and thinner films as annotated by stars.

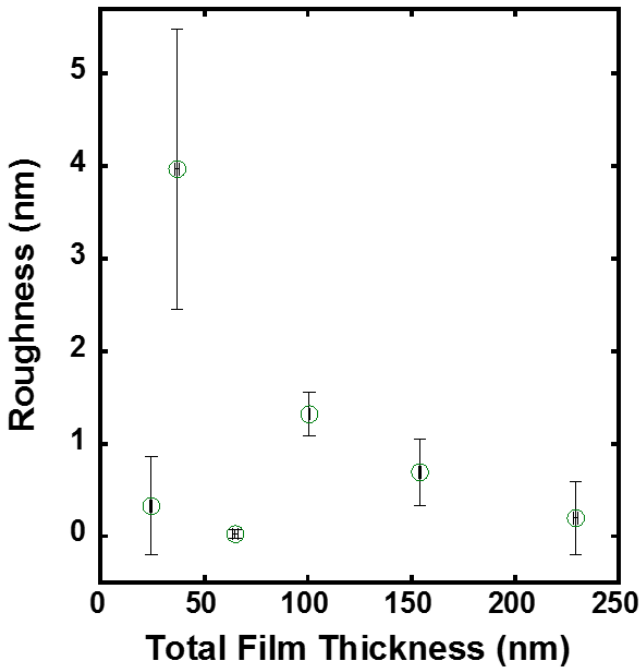

Figure 15. Mean surface roughness shown with standard deviation bars for regiorandom P3HT films of various thickness as determined using the two-layer anisotropic model.

The two-layer anisotropic model with roughness included was also used to characterize the thickness of the bottom layer. Figure 16a shows the bottom thickness plotted vs. the total film thickness. Models for the 154 nm and 230 nm films converge on a bottom layer of approximately 4 nm. This buried aligned layer thickness is in close agreement with the 4.5 nm predicted by Zhang et. al.[1] When roughness is not included in the model, these results are essentially unchanged as shown in Figure 16b.

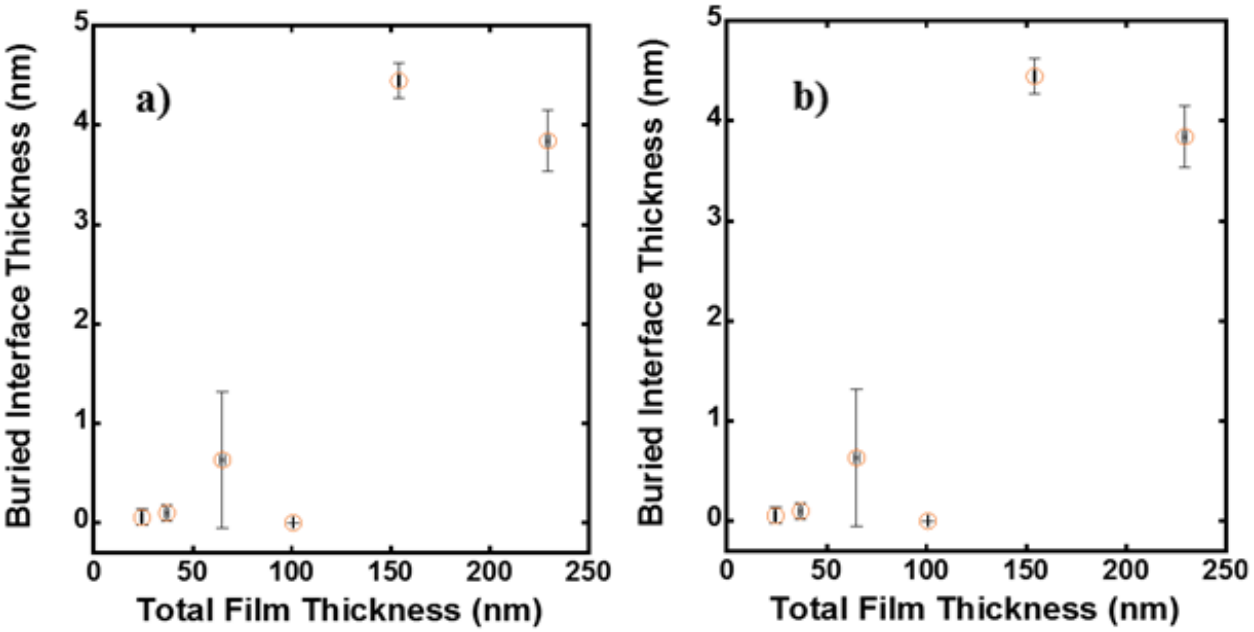

Figure 16. Aligned buried interface thickness shown with standard deviation bars for regiorandom P3HT films of various thickness as determined using a two-layer anisotropic model

Aligned buried interface thickness shown with standard deviation bars for regiorandom P3HT films of various thickness as determined using a two-layer anisotropic ellipsometry model that a) accounts for surface roughness and b) does not account for surface roughness. The thickest two sets of samples in both models have a buried interface thickness of about 4 nm.

The inclusion of the aligned bottom layer lowers the weighted MSE in all 154 nm and 230 nm thick sample models. For the 154 nm samples, MSE decreases between 9.8% and 1.2% depending on the data set. The mean decrease is 5.4% with a standard deviation of 3.2% For the 230 nm samples, MSE decreases between 1.4% and 0.8% depending on the data set. The mean decrease is 1.1% with a standard deviation 0.3%. The MSE decrease justifies the inclusion of an aligned layer in the model. Table 5 summarizes how the mean birefringence, interface layer thickness, and MSE change between one and two layer anisotropic models for the 154 nm films.

Table 5. Comparison of one and two layer anisotropic models for 154 nm films

Model	Roughness (nm)	Mean 1100 nm birefringence	Mean buried interface thickness (nm)	Mean Weighted MSE
One-layer with roughness	0.70	0.0028	0	4.81
One-layer without roughness	0	0.0019	0	4.82
Two-layer with roughness	0.69	0.0006	4.45	4.58
Two-layer without roughness	0	-0.0003	4.45	4.60

Parameter uniqueness fits were run for the bottom layer thickness in the 154 nm and 230 nm samples. Figure 17 shows sample results at each thickness.

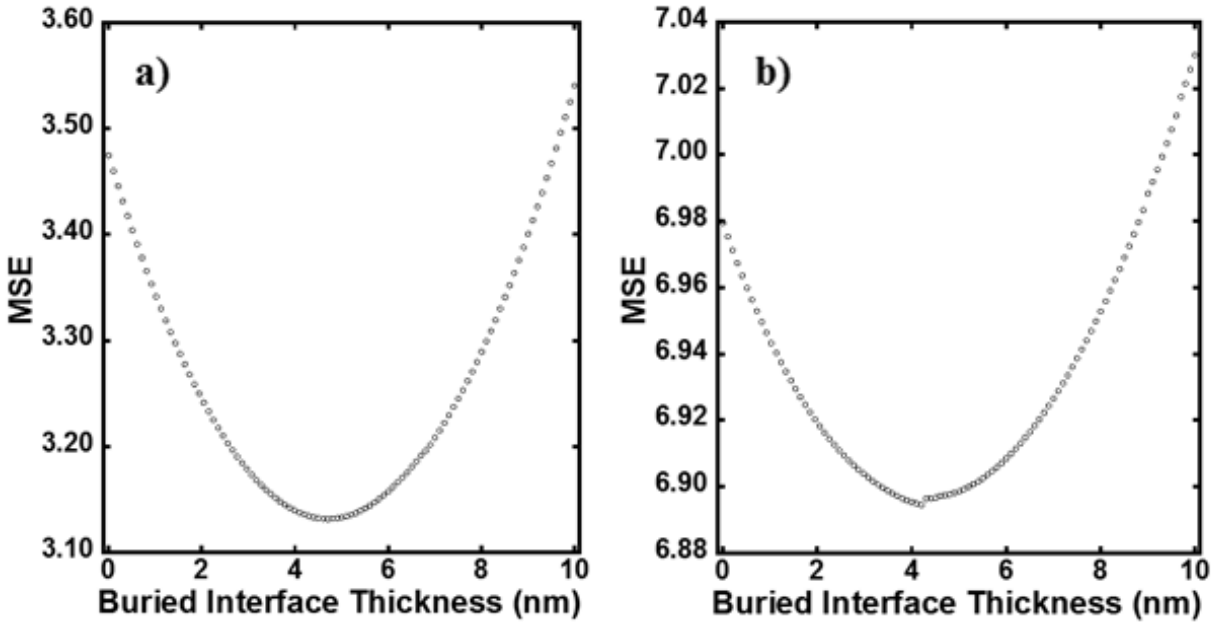

Figure 17. Parameter uniqueness tests on the buried interface thickness

Parameter uniqueness tests on the buried interface layer thickness for a) a 155 nm film and b) a 230 nm film fit with the two-layer anisotropic model that accounts for surface roughness. The presence of an obvious minimum MSE is evidence that the thicknesses are meaningful.

The test shows that the models do exhibit sensitivity to the interface thickness, as the fits clearly reach a minimum weighted MSE. When considered with the overall MSE decrease for

the two layer fits, this provides strong evidence that the ellipsometry results are meaningful rather than over fitting of data.

Although there is no meaningful MSE difference between models with and without surface roughness, the models that do account for it are likely most rigorous. These films are not expected to be perfectly smooth, and the inclusion of roughness eliminates the possibility that the model is falsely assigning optical response from roughness to the aligned layer. Accounting for surface roughness only adds one degree of freedom to the model.

The correlation coefficients between the top and bottom layer thickness in the two-layer models are greater than 0.99, which indicate that the models are more sensitive to the overall thickness of the sample than to the thickness of the bottom layer alone. Correlation is a consequence of ellipsometry data analysis being an indirect process, and is not unexpected when one parameter has a disproportionate impact on the total optical response of the film.[15] In this case, the total thickness of the film, which is nearly the bulk or "top" thickness parameter, has a larger effect on optical response than the much thinner aligned layer.

A two-layer model with an isotropic top and anisotropic bottom was fit to all of the data to see if the anisotropic top assumption is critical to the aligned layer thickness results. As in the two-layer anisotropic model, the top layer optical response and the thickness of both layers was was allowed to fit while the bottom anisotropic layer was fixed with the derived regioregular P3HT optical properties. Figure 18 shows the bottom layer thicknesses for this model.

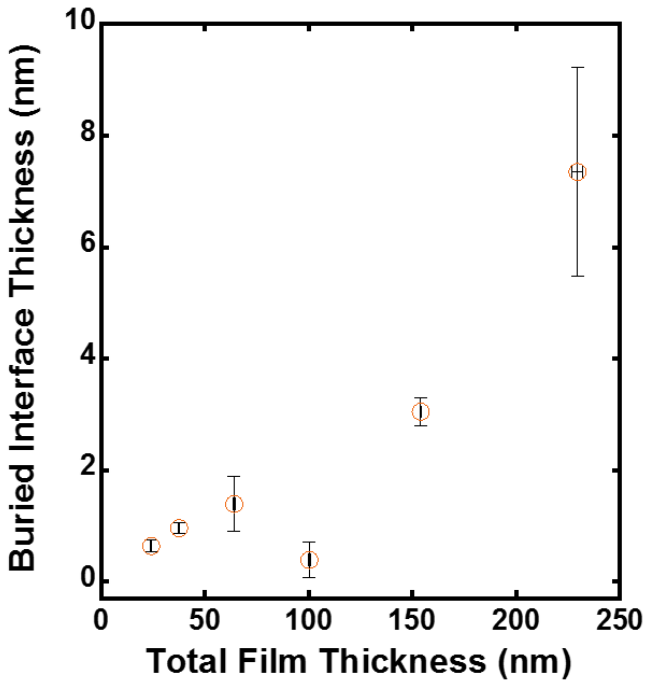

Figure 18. Aligned buried interface thickness shown with standard deviation bars for regiorandom P3HT films of various thickness as determined using a two-layer isotropic model

Aligned buried interface thickness shown with standard deviation bars regiorandom P3HT films of various thickness as determined using a two-layer isotropic top ellipsometry model that does not account for surface roughness. Although the fit quality is worse for this model than for the two-layer anisotropic model, the results are similar.

The thinnest four samples now exhibit a bottom layer ranging from approximately 0.4 nm to 1.4 nm in thickness. However, the thicker 154 nm and 230 nm samples are still found to have significantly thicker bottom layers, which is consistent with the two-layer anisotropic results. The weighted MSE values for fits with the two-layer isotropic top model are significantly higher than the two-layer anisotropic model.

The two-layer anisotropic model was determined to best fit and therefore best describe the optical response of the regiorandom P3HT films. When fit with the version of this model that considers the possibility of surface roughness, 154 nm and 230 nm thick films exhibit a mean

bottom layer thickness of 4.4 nm and 3.8 nm respectively. This is consistent with the prediction made by Zhang et. al. Thinner films exhibit greatly reduced mean bottom layer thicknesses.

The 38 nm, 66 nm, and 101 nm films have statistically greater top layer 1100 nm mean birefringence than the 154 nm and 230 nm films. It is possible that the approximately 4 nm thick aligned layer only forms or can only be detected in thicker films because the thinner films exhibit a greater degree of alignment overall.

Chapter 4: Conclusion

Regiorandom P3HT films of various total thickness were prepared and studied with spectroscopic variable angle Mueller matrix ellipsometry in order to characterize predicted alignment at the buried substrate interface. Several different models were developed to analyze the data, including a two-layer anisotropic model in which optical properties derived from regioregular P3HT were used to simulate the potential optical response from a bottom aligned layer. Birefringence and bottom layer thickness were measured in order to study changes with overall film thickness. Birefringence was used to measure relative alignment in the samples and propose an explanation for the buried interface thickness results.

Both one and two layer models in which the bulk of the film is modeled as anisotropic were found to fit the data better than models in which the bulk of the film is modeled as isotropic. In these anisotropic models, transparent region birefringence was statistically significantly higher in thin films than in thicker films. This trend is observed regardless of if roughness is included in the models or not.

A two-layer model in which the top layer is anisotropic and the bottom layer has the same anisotropic optical properties as regioregular P3HT was found to best fit the data. Using this model, the 154 nm and 230 nm samples were found to have a mean bottom layer thickness of 4.4 nm and 3.8 nm respectively, whereas thinner samples were found to have a mean bottom layer thickness of no more than 0.7 nm. The results remain nearly the same regardless of if roughness is included in the model or not. This result provides experimental evidence for the 4.5 nm aligned layer predicted by Zhang et. al for P3HT films. It is possible that this technique is not sensitive enough to detect the aligned layer in thinner films, or that thinner films align throughout rather than only at the interface due to interactions not considered by Zhang et. al.

Appendix: Ellipsometry Modeling

This appendix is designed to help the reader understand the process used to model ellipsometry data. Figures are screenshots from CompleteEase, the modeling software used in this thesis.

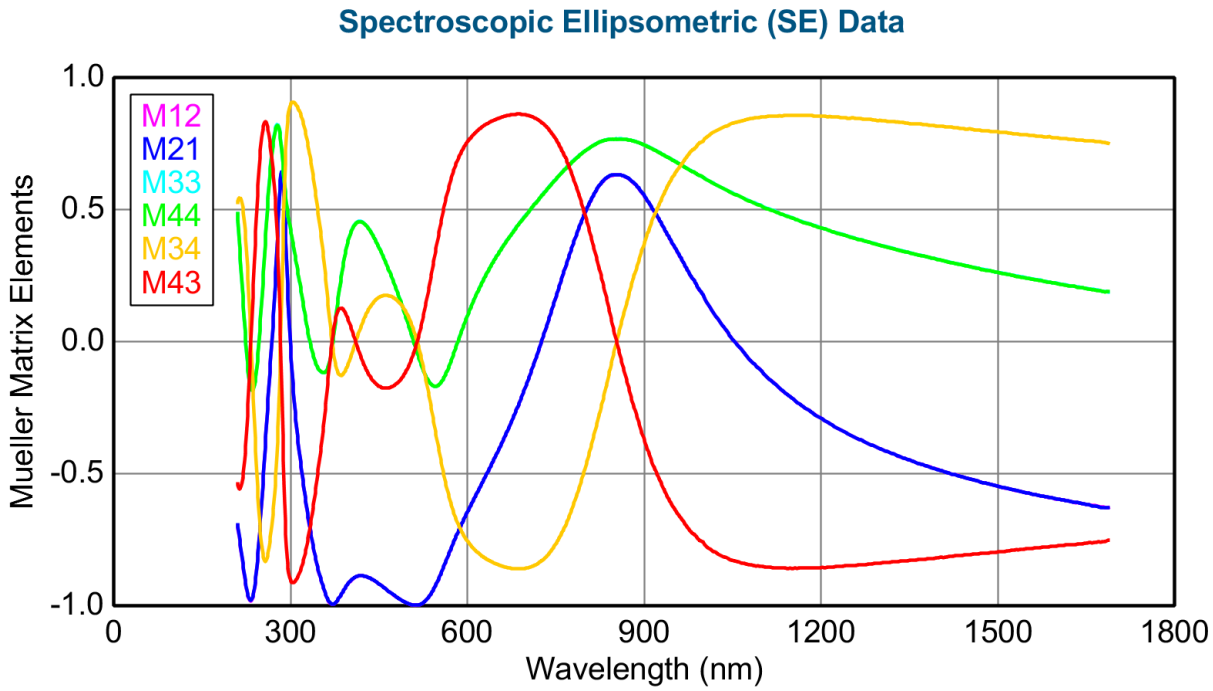

Example of raw diagonal MM elements data from a single angle of incidence. In standard ellipsometry this would be equivalent to the NCS plot, which is a transformation of the psi and delta values that describe the change in the polarization state of incident light caused by the sample.

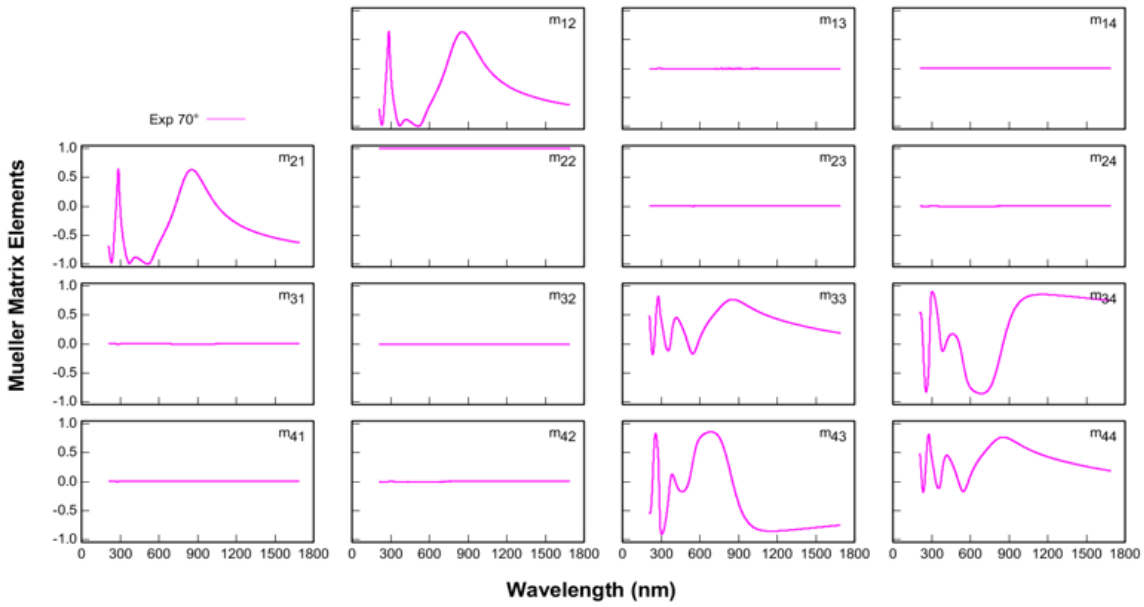

Raw data for 15 MM elements at one angle of incidence. M_{11} is not shown as all other elements are normalized to this element. The non-zero and non-one elements are most critical to modeling this system

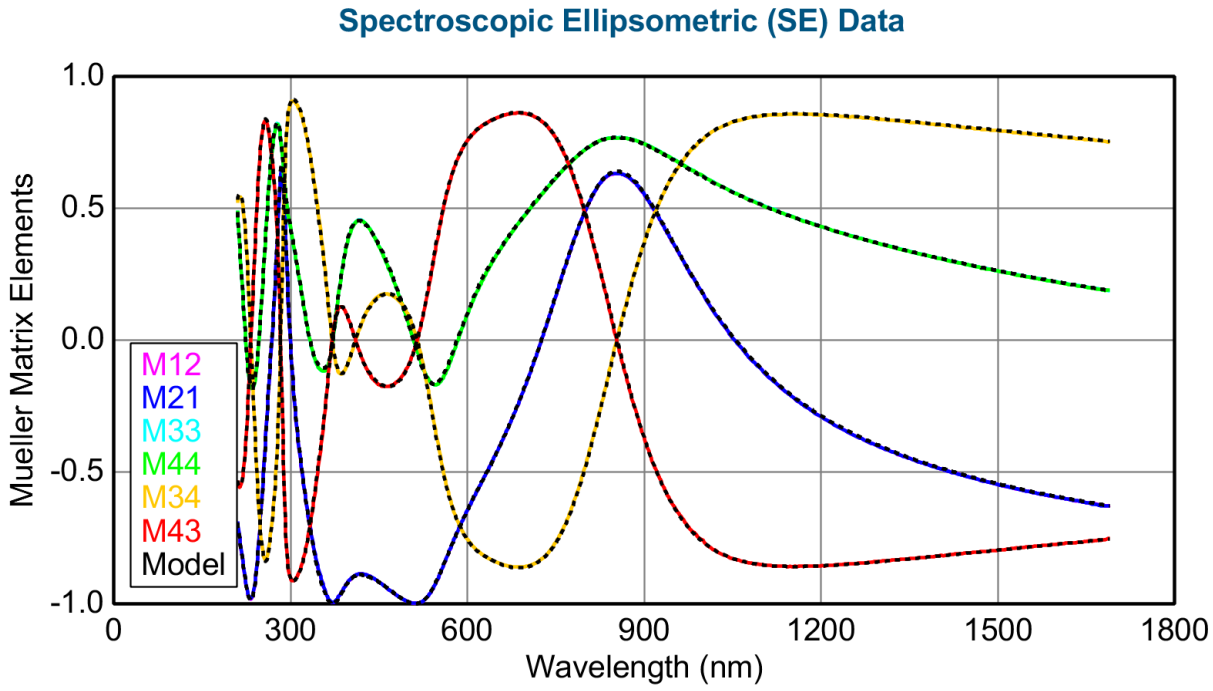

Ellipsometry data fit with a rigorous model in CompleteEase. Over the full spectral range the model clearly fits the raw data and closer inspection is needed to evaluate the quality as compared to other plausible models.

Layer Commands: Add Delete Save
Include Surface Roughness = OFF
- Layer # 4 = EMA-coupled Thickness # 4 = **0.81 nm** (fit)
  # of Constituents = 2
  - Material 1 = Coupled
    Coupled to Layer # = 3 (Biaxial)
  Material 2 = Void
  EMA % (Mat 2) = 50.0
  depolarization = 0.333 Analysis Mode = Bruggeman
- Layer # 3 = Biaxial Thickness # 3 = **149.51 nm** (fit)
  Type = Uniaxial
  Optical Constants: Difference Mode = OFF
  - Ex = allRRa16butreally22_std
    Add Oscillator Show Dialog Fast Gaussian Calc = ON
    Einf = **1.343** (fit)
    UV Pole Amp. = 0.000 UV Pole En. = 0.00
    IR Pole Amp. = 0.000
    Fit All Clear All Add Amp. Add Br. Add En.
    1: Type = Tauc-Lorentz Amp1 = **20.5433** (fit)
    Br1 = **4.818** (fit) Eo1 = **10.210** (fit) Eg1 = **2.120** (fit) Common Eg = OFF
    2: Type = Tauc-Lorentz Amp2 = **0.5194** (fit)
    Br2 = **0.583** (fit) Eo2 = **4.532** (fit) Eg2 = **2.740** (fit) Common Eg = OFF
    3: Type = Gaussian Amp3 = **0.686492** (fit) Br3 = **0.3706** (fit) En3 = **2.560** (fit)
    4: Type = Gaussian Amp4 = **0.404509** (fit) Br4 = **0.8276** (fit) En4 = **3.256** (fit)
    5: Type = Gaussian Amp5 = **0.778166** (fit) Br5 = **0.5180** (fit) En5 = **2.821** (fit)
  - Ez = Gen-Osc
    Add Oscillator Show Dialog Fast Gaussian Calc = ON
    Einf = **1.407** (fit)
    UV Pole Amp. = 0.000 UV Pole En. = 0.00
    IR Pole Amp. = 0.000
    Fit All Clear All Add Amp. Add Br. Add En.
    1: Type = Gaussian Amp1 = **1.026852** (fit) Br1 = **0.7574** (fit) En1 = **2.723** (fit)
    2: Type = Gaussian Amp2 = **0.216601** (fit) Br2 = **1.2471** (fit) En2 = **3.480** (fit)
    3: Type = Tauc-Lorentz Amp3 = **35.8158** (fit)
    Br3 = **8.714** (fit) Eo3 = **9.745** (fit) Eg3 = **3.491** (fit) Common Eg = OFF
    4: Type = Gaussian Amp4 = **0.205146** (fit) Br4 = **0.5400** (fit) En4 = **4.559** (fit)
  Euler Angles: Phi = 0.00 Theta = 0.00
- Layer # 2 = Biaxial Thickness # 2 = **4.46 nm** (fit)
  Type = Uniaxial
  Optical Constants: Difference Mode = OFF
    Ex = X_common
    Ez = Z_common
  Euler Angles: Phi = 0.00 Theta = 0.00
Layer # 1 = NTVE_JAW Native Oxide = 2.33 nm
Substrate = SI_JAW
Angle Offset = 0.00

Fully set-up model that has converged on a reasonable result. Bolded values are fit. All fit parameters are positive numbers of expected magnitude. Gaussian and Tach-Lorentz curves are used as KK consistant oscillators to model the optical properties of various layers. Layer #1 is the native oxide thickness of the silicon substrante. Layer #2 is the buried interface layer with optical properties set to those of regioregular P3HT. Layer #3 is the bulk of the film modeled as uniaxial and isotropic. Layer #4 is surface roughness modeled as an EMA of void and the bulk film.

a)

MSE = 3.628
Thickness # 4 = 0.81±0.044 nm
Thickness # 3 = 149.51±0.112 nm
Einf = 1.343±0.0209
Amp1 = 20.5433±1.10945
Br1 = 4.818±0.2383
Eo1 = 10.210±0.1144
Eg1 = 2.120±0.0905
Amp2 = 0.5194±0.06468
Br2 = 0.583±0.008106
Eo2 = 4.532±0.003241
Eg2 = 2.740±0.1209
Amp3 = 0.686492±0.0705578
Br3 = 0.3706±0.00681
En3 = 2.560±0.003882
Amp4 = 0.404509±0.0210217
Br4 = 0.8276±0.03089
En4 = 3.256±0.0277
Amp5 = 0.778166±0.0669749
Br5 = 0.5180±0.02523

b)

MSE = 13.450
Thickness # 4 = -1.00±0.152 nm
Thickness # 3 = 144.51±0.312 nm
Einf = 1.004±0.0396
Amp1 = 60.0164±7.15247
Br1 = 34.476±2.3679E-08
Eo1 = 14.868±1.2449
Eg1 = 2.838±0.0196
Amp2 = 0.001000±0.89935
Br2 = 128.904±1.1104E-09
Eo2 = 0.00010000±8.9503
Eg2 = 5.180±5.0163E-10
Amp3 = 1.067339±0.0222124
Br3 = 0.4106±0.00424
En3 = 2.579±0.001258
Amp4 = -31.887149±6.5805E-08
Br4 = 0.000±0.11382
En4 = 15.000±7.1526E-07
Amp5 = 0.824470±0.0100402
Br5 = 0.7041±0.01006

Model outputs for a) a reasonable result in which the MSE is low. All numbers are of the expected order of magnitude, positive, and have error bars lower than the value itself. b) An unacceptable model in which MSE is moderately high. Parameters are unphysically negative, large, and have error bars larger than the value itself.

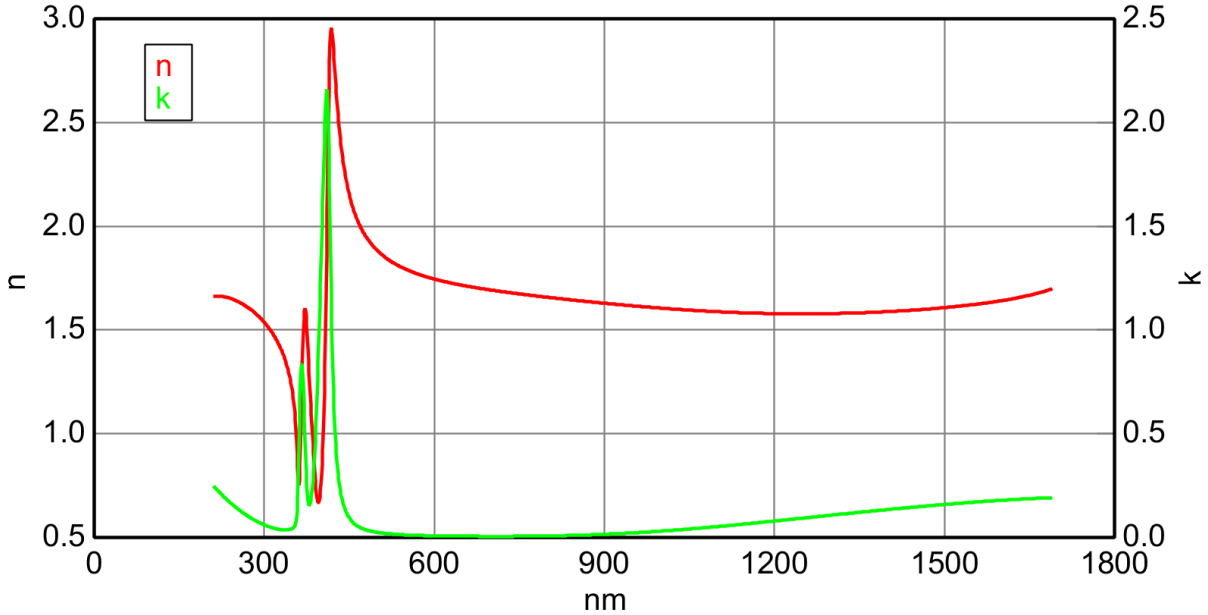

Unrealistic optical properties derived from a model. In some cases, such an unphysical result can be derived even for an otherwise acceptable output. A broad absorption peak in the UV-visible range is expected and no absorption is expected above 900 nm. In this case, the fit can be ruled out. See Figure 5 and Figure 6 for examples of acceptable properties.

BIBLIOGRAPHY

1. Zhang, W.; Gomez, E. D.; Milner, S. T. *Macromolecules* **2016**, *49* (3), 963–971.
2. Morse, D. C.; Fredrickson, G. H. *Physical Review Letters* **1994**, *73* (24), 3235–3238.
3. Kline, R. J.; Mcgehee, M. D.; Toney, M. F. *Nature Materials* **2006**, *5* (3), 222–228.
4. Leolukman, M.; Kim, S. H. *Langmuir* **2005**, *21* (2), 682–685.
5. Li, J.; Park, J. K.; Moore, R. B.; Madsen, L. A. *Nature Materials* **2011**, *10* (7), 507 511.
6. Hamley, I. W. *Soft Matter* **2010**, *6* (9), 1863.
7. Zhao, B.; He, G.; Hamouti, I. E.; Gao, L.; Liu, Y.; Deng, R.; Yan, X. *International Journal of Hydrogen Energy* **2017**, *42* (15), 10228–10237.
8. Kierfeld, J.; Baczynski, K.; Gutjahr, P.; Lipowsky, R.; Garay, O. J.; García-Río Eduardo; Vázquez-Lorenzo Ramón. *AIP Conference Proceedings* **2008**.
9. Chen, J. Z. Y.; Sullivan, D. E. *Macromolecules* **2006**, *39* (22), 7769–7773.
10. Chen, J. Z. Y.; Sullivan, D. E.; Yuan, X. *Macromolecules* **2007**, *40* (4), 1187–1195.
11. Ivanov, V. A.; Rodionova, A. S.; An, E. A.; Martemyanova, J. A.; Stukan, M. R.; Müller, M.; Paul, W.; Binder, K. *Physical Review E* **2011**, *84* (4).
12. Xiao, M.; Jasensky, J.; Zhang, X.; Li, Y.; Pichan, C.; Lu, X.; Chen, Z. *Physical Chemistry Chemical Physics* **2016**, *18* (32), 22089–22099.
13. Arruda, E. M.; Przybylo, P. A. *Polymer Engineering and Science* **1995**, *35* (5), 395–402.
14. Beiermann, B. A.; Kramer, S. L. B.; May, P. A.; Moore, J. S.; White, S. R.; Sottos, N. R. *Advanced Functional Materials* **2013**, *24* (11), 1529–1537.

15. Garcia-Caurel, E.; Martino, A. D.; Gaston, J.-P.; Yan, L. *Applied Spectroscopy* **2013**, *67* (1), 1–21.

16. Tompkins, H. G.; Hilfiker, J. N. *Spectroscopic ellipsometry: practical application to thin film characterization*; Momentum press: New York, 2016.

17. Campoy-Quiles, M.; Etchegoin, P. G.; Bradley, D. D. C. *Physical Review B* **2005**, *72* (4).

18. Geoghegan, M.; Hadziioannou, G. *Polymer electronics*; Oxford University Press: Oxford, 2014.

19. Thurn-Albrecht, T.; Thomann, R.; Heinzel, T.; Hugger, S. *Colloid & Polymer Science* **2004**, *282* (8), 932–938.

Academic Vita of Bryan Smith

bhs5097@psu.edu

Education

Bachelor of Science in Chemical Engineering
Pennsylvania State University, University Park, PA
Schreyer Honors College
Honors in Chemical Engineering
Minors: Electronic and Photonic Materials, History

Work Experience

Analytical Services Intern, 5/2015-7/2017
- LORD Corporation, Erie, PA
- Materials characterization, chemical testing, chromatography

Lead Orientation Student Coordinator, 11/2015-4/2018
- Penn State Global Programs, University Park, PA
- International student orientation, student manager, global engagement

Research

Undergraduate thesis, 1/2015-4/2018
- Dr. Enrique Gomez, Penn State Chemical Engineering, University Park, PA
- Polymer thin-film characterization, ellipsometry, chain alignment

DAAD RISE, 5/2016-7/2016
- Friedrich Alexander University Erlangen-Nuremburg, Germany
- OLED fabrication, dielectric mirror printing, international experience

PPG Undergraduate Research Fellow, 6/2015-8/2015
- Dr. Enrique Gomez, Penn State Chemical Engineering, University Park, PA
- Polymer synthesis, OPV active layers, industry presentation

Honors and Awards

Larry Duda Undergraduate Research Award, 4/2016
PPG Undergraduate Research Fellowship, 6/2015
President's Freshman Award, 3/2015
McWhirter Undergraduate Scholarship, 7/2014